Title

Correlation between the elastic modulus of anterior cruciate ligament (ACL) and quantitative ultrashort echo time (UTE) magnetic resonance imaging.

Journal

Journal of Orthopaedic Research, 40(10)

Authors

Hananouchi, Takehito

Ma, Yajun

Namiranian, Behnam

et al.

Publication Date

2022-10-01

DOI

10.1002/jor.25266

Peer reviewed

HHS Public Access

Author manuscript

J Orthop Res. Author manuscript; available in PMC 2022 October 01.

Correlation between the elastic modulus of anterior cruciate ligament (ACL) and quantitative ultrashort echo time (UTE) magnetic resonance imaging

Saeed Jerban[1,†,*], **Takehito Hananouchi**[2,†], **Yajun Ma**[1], **Behnam Namiranian**[1], **Erik W. Dorthe**[3], **Jonathan H. Wong**[4], **Niloofar Shojaeiadib**[4], **Mei Wu**[1], **Jiang Du**[1], **Darryl D'Lima**[2,*], **Christine B. Chung**[1], **Eric Y. Chang**[4,1,*]

[1]Department of Radiology, University of California San Diego, San Diego, CA 92093, USA

[2]Department of Mechanical Engineering, Osaka Sangyo University, Daito, Osaka, Japan

[3]Shiley Center for Orthopedic Research and Education at Scripps Clinic, La Jolla, CA 92037, USA

[4]Research Service, VA San Diego Healthcare System, San Diego, CA 92161, USA

Abstract

Conventional magnetic resonance imaging (MRI) often acquires no signal in anterior cruciate ligament (ACL) due to the short apparent transverse relaxation time of ACL. Ultrashort echo time (UTE) MRI is capable of imaging ACL with high signal which enables quantitative ACL assessment. This study aimed to investigate the correlations of the mechanical and microstructural properties of human ACL specimens with quantitative three-dimensional UTE Cones (3D-UTE-Cones) MRI measures. ACL specimens were harvested from cadaveric knee joints of thirteen (50.9±21.1 years old, 11 males and 2 female) donors. Specimens were scanned using a series of quantitative 3D-UTE-Cones T_2* (UTE-T_2*), T_1 (UTE-T_1), Adiabatic $T_{1\rho}$ (UTE-Adiab-$T_{1\rho}$), and magnetization transfer (UTE-MT) sequences in a wrist coil on a clinical 3T scanner. ACL elastic modulus was measured using a uniaxial tensile mechanical test. Histomorphometry analysis was performed to measure the average fascicle specific surface, fascicle size, and number of cells per unit area. Spearman's rank correlations of UTE-MRI biomarkers with mechanical and histomorphometry measures were investigated. The elastic modulus of ACL showed significant

[*]**Corresponding author: Darryl D'Lima,** Shiley Center for Orthopedic Research and Education at Scripps Clinic, La Jolla, CA 92037, USA, ddlima@scripps.edu , Phone: +1 858 554 7011, Fax: +1 858 554 7011; **Eric Y. Chang,** Research Service, VA San Diego Healthcare System, 3350 La Jolla Village Drive, San Diego, CA 92161, USA, ericchang.2@va.gov, Phone: +1 858 246 2248, Fax: +1 888 960 5922;**Saeed Jerban**, Department of Radiology, University of California, San Diego, 9500 Gilman Dr., La Jolla, CA 92093, USA, sjerban@ucsd.edu, Phone: +1 858 246 2248, Fax: +1 888 960 5922.

Author Contributions Statement: Saeed Jerban had contributions to design, experiment, MRI scans, data analyses and manuscript drafting. Takehito Hananouchi had contributions to design, experiment, mechanical measurements, and data analyses. Yajun Ma developed the MT-UTE MRI sequence and helped on the data interpretation. Behnam Namiranian helped in performing the experiments and MRI data analysis. Erik W. Dorthe contributed to mechanical measurements and interpretations. Jonathan H. Wong and Niloofar Shojaeiadib carried out the histology studies and analysis. Mei Wu helped ACL dissection and sample preparation. Jiang Du, Darryl D'Lima, Christine B. Chung, and Eric Y. Chang helped designing the study, supervising all steps of the project and data analysis, and reviewing the manuscript.

All authors have read and approved the final submitted manuscript

[†]Saeed Jerban and Takehito Hananouchi contributed equally to this work.

6.Conflict of interest statement

The authors have no conflicts of interest to declare.

moderate correlations with UTE-Adiab-$T_{1\rho}$ (R=−0.59, P=0.01), macromolecular fraction (MMF) from MT modeling (R=0.54, P=0.01), magnetization transfer ratio (MTR) (R=0.53, P=0.01), UTE-T2* (R=−0.53, P=0.01), and average fascicle specific surface (R=0.54, P=0.01). UTE-MRI showed non-significant correlations with histomorphometry measures. UTE-MRI biomarkers may be useful non-invasive tools for the ACL mechanical assessment.

Keywords

Anterior cruciate ligament; quantitative MRI; UTE; magnetization transfer; Adiab-$T_{1\rho}$; mechanical properties

1. Introduction

The anterior cruciate ligament (ACL) is a key musculoskeletal tissue in the human knee joint that constrains the relative motion between the femur and the tibia [1]. ACL is comprised of highly structured collagen fibers predominantly parallel to the long axis of the ligament [2,3].

ACL injury or overuse may alter the organized collagen fiber structure and can results in fiber disruption [1,4]. The injury-related changes of ligaments often can be detected semi-quantitatively using conventional magnetic resonance imaging (MRI). Conventional MRI has been used in several studies to assess the structure of ligaments and tendons [2,5-8]. Basically, MRI signal intensity of an injured or recovering ligament is higher than that of intact tissues. Clinical MR signal intensity has been used in various studies to evaluate ACL graft maturity following ACL reconstruction surgeries [9,10,19,11-18]. The assessment of ligaments using MR signal intensity is highly challenging as the signal intensity in MRI images depends on various factors such as the scanner and coil specifications, coil positioning, acquisition parameters, reconstruction algorithms, and signal normalization.

Quantitative MRI such as transverse relaxation time (T2 or T2*) and spin lock relaxation time (T1ρ) have been also used for ACL assessment [20-26]. Quantitative MRI provides more robust assessments compared with the simple MR signal intensity. T2* has shown correlations with mechanical [25] and histological properties of healing ACL grafts in animal models [24] and with mechanical properties of intact cadaveric ACL specimens [26]. T1ρ relaxation is the relaxation that occurs after the application of a relatively long-duration on-resonance RF pulse in order to “spin-lock” the magnetization vector into a rotated frame [2,27,28]. T1ρ relaxation time is always higher than T2 relaxation time. The T1ρ biomarker has been hypothesized to be sensitive to slow-motion interactions between protons of constrained water molecules and those of associated macromolecules in the extracellular matrix of musculoskeletal tissues [2,27,28]. Although T1ρ has been used for cartilage structural and mechanical properties [29-32], to our knowledge it has not been used for assessment of the native ACL.

A large portion of ligament tissues possess short T2 values and therefore cannot be assessed using conventional MRI sequences that use long TEs [33]. Ultrashort echo time (UTE) MRI sequences can image short T2 musculoskeletal tissues with high signal [3,34-37]. Nevertheless, the regular UTE biomarkers, such as UTE T1ρ and T2, and bi-component T2* analysis

are sensitive to the orientation angle of the tissue relative to the scanner bore axis (B0) as explained by the magic angle effect [38-40].

A novel T1ρ sequence has been recently developed using an adiabatic spin-lock pulse cluster followed by 3D UTE Cones data acquisition (3D UTE-Adiab-T1ρ) [35]. Adiabatic pulses provide a robust spin-lock in the rotated magnetization frame with a highly reduced sensitivity to B1 inhomogeneity. Recent studies have shown that the 3D UTE-Adiab-T1ρ is an demonstrate low-sensitivity to the magic angle effect [41-43]. UTE-MRI combined with magnetization transfer (UTE-MT) has also been recently proposed as an orientation-insensitive technique to quantify the macromolecular content in the MSK tissues [44,45]. UTE-MT modeling provides multiple parameters, including macromolecular fraction (MMF), macromolecular relaxation time (T2mm), and exchange rates [44,45]. Recent studies also demonstrate that UTE-MT modeling is insensitive to the magic angle effect [44,46], supporting its potential for effective unbiased ACL assessment. However, the relationships between these orientation-insensitive techniques (UTE-MT and Adiab-T1ρ) and the mechanical and microstructural properties of ACL have not yet been investigated.

The main objective of the present study was to investigate the correlations of a panel of quantitative 3D UTE Cones MRI techniques (UTE-Adiab-T1ρ, UTE-T2*, UTE-T1, UTE-MT) with the mechanical and microstructural properties of human ACL specimens. It should be noted that the magic angle effect of the applied UTE-MRI techniques was investigated in prior studies [42-44,46]. UTE-MRI-based estimation of ACL mechanical and microstructural properties can potentially open a new venue to improve ACL injury detection or graft monitoring after reconstruction.

2. Materials and Methods

2.1. Sample preparation

ACL specimens were dissected from thirteen fresh-frozen knee cadaveric joints from eleven male and two female donors (50.9±21.1 years old at the time of death). Frozen knee joints were provided by a non-profit whole-body donation company (United Tissue Network, Phoenix, AZ). The average length of specimens was 25.1±2.9 mm. The average volume of the specimens was 893±342 mm3. Length and volume values for all specimens are presented in Table 1S, in Supplemental Materials. Figure 1A shows a representative harvested ACL specimen from a 57-year-old male donor. All specimens were arranged around a cylindrical plastic tube (i.e., a section of a standard 30-ml syringe) as shown in Figure 1B for MRI imaging. The time passed from the dissection to the scanning session differed from 3 hours to 7 hours approximately for different specimens. Although the dissected ACL specimens were kept in wet gauze to avoid large dehydration, they were soaked in phosphate-buffered saline (PBS) for 2 hours before scanning in order to ensure similar levels of hydration in all specimens.

2.2. Quantitative UTE-MRI

The UTE-MRI scans were performed on a 3T MRI scanner (MR750, GE Healthcare Technologies, WI, USA) using a transmit/receive wrist coil (Mayo Clinic BC-10, two

channels, Transmit/Receive birdcage coil). Specimens were placed in a plastic container filled with perfluoropolyether (Fomblin, Ausimont, NJ, USA) to minimize dehydration and susceptibility artifacts during MRI scans. The container was positioned vertically inside the wrist coil to ensure ACL alignment perpendicular to B0. All MRI images were acquired in the coronal plane.

Four following sets of 3D UTE Cones MRI sequences were performed, 1) 3D UTE Cones T2* sequence to measure T2* values, 2) actual flip angle imaging with variable TR (AFI-VTR)-based 3D UTE Cones sequence to measure T1 values [47], 3) 3D UTE Cones Adiab-T1ρ sequences to measure T1ρ values, and 4) 3D UTE Cones MT sequences with three saturation pulse power levels at five different frequency offsets for MT ratio (MTR) measurements and two-pool MT modeling [44,45]. Data acquisition parameters for the four quantitative UTE-MRI protocols are presented in Table 1. Features of the 3D UTE Cones sequence have been described in previous studies [48].Details of the 3D UTE-Adiab-T1ρ and two-pool UTE-MT modeling are given in earlier studies [35,44,45]. Figure 1C shows a UTE-MRI (TE=0.032 ms, TR=500 ms, and FA=10°) image of the thirteen ACL specimens in the plastic container filled with Fomblin (with no MRI signal) imaged in the coronal plane.

UTE-MRI biomarkers were calculated in three representative slices at the middle of each ACL specimen (volume of interest, VOI is indicated in Figure 1A) within global regions of interest (ROIs) covering the entire width of the specimens. For each slice, average signal values within the ROI were used for the T2*, T1, and T1ρ fittings, and for the MT-modeling. Then the values for three slices were averaged to obtain the average value for each specimen.

Repeatability of the UTE-MT-MRI measures have been investigated in an earlier study on bone where an average coefficient of variation (i.e., standard deviation/average) below 2% was observed 55. Repeatability level of other UTE-MRI measures are expected to be similar as similar scanning and analysis steps are being used.

Single-component exponential fitting models were used to measure T_2*, T_1, and Adiab-$T_{1\rho}$ relaxation times. The acquired UTE-MT dataset with three saturation pulse power levels and five frequency offsets was used in two-pool MT modeling to calculate MMF and T_2mm [44]. MTR values were also measured using the MT dataset. All UTE-MRI measurements and models were performed using in-house developed codes in MATLAB (version 2017, The Mathworks Inc., Natick, MA, USA).

2.3. Tensile mechanical test

After MRI scans, specimens were washed with PBS before running mechanical tests. The mechanical setup with a mounted ACL specimen is shown in Figure 1D. Both ends of the specimens were trimmed into 7×5 mm2 cross-sections approximately (the gripper space dimension) and then mounted on the grippers of an in-house developed benchtop uniaxial loading device. Trimming mainly involved the ligament membrane and the epilligament layer. Other portion of specimens were kept intact. On average, 5 mm of the ACL lengths were mounted in each gripper. The original distance between the fixed and actuated gripper was set to 15 mm. After initial alignment and preloading to straighten the specimens (steps

of 0.005-N tension were applied for 5s periods up to the time the sample held 0.02 N as preload for 20s), a 1-mm tensile displacement was applied at 2 mm/min rate and the applied force was recorded. Average maximum mechanical stress was calculated as the maximum force (at 1mm displacement) divided by ACL cross-section. The maximum strain for all specimens was 0.067 (i.e., 1 mm / 15 mm). The average tensile elastic modulus was calculated as the average maximum stress divided by the average maximum strain.

2.4. Histology and histomorphometry

To assess microstructure of the ACL specimens through histomorphometric analyses, a 5-mm thick cross-sectional slice from the mid-third of the ACL (Figure 1A) was cut and underwent histological analysis. These ACL slices were fixed in zinc-formalin fixative (Anatech, Battle Creek, MI, USA) for three days at room temperature. The fixed samples were dehydrated and then embedded in paraffin. A set of 5-μm axial sections of ACLs were cut and alternating slides stained with Alcian blue/periodic-acid-schiff (AB/PAC). Two representative histology sections, 1-mm apart, were selected per ACL specimen by an experienced histologist blinded to MRI and mechanical test results. Selected slices were imaged using a virtual microscopy scanner (Axio Scan.Z1, Carl Zeiss, Jena, Germany) for the fascicle structural analysis of ligament samples. ROIs for histomorphometry analysis were selected manually covering entire cross-section of the specimens while avoiding edges (epiligament…) and regions with staining or cutting artifacts.

Pixels belonging to fascicles (colorful pixels in Figure 3) were segmented from the void space in the histology images using semi-automatic color-based segmentation algorithms available in the MATLAB image processing toolbox. Fascicles were considered as the secondary collagen fiber bundles in the ACL specimens. Number of pixels in fascicles and number of pixels in the periphery of fascicles were counted using image processing operations performed on the segmented images. Average fascicle specific surface was calculated as the number of periphery pixels divided by the total number of pixels in the fascicles. The fascicle size (thickness) at each pixel was defined as the diameter of the largest covering circle, an oft-used definition in the literature, utilizing the distance transform on the segmented images. Average fascicle size was calculated by averaging the local fascicle size values over all segmented pixels. Cells in the histology images were segmented and counted using a color-based segmentation algorithm in the MATLAB image processing toolbox.

Repeatability of the histomorphometry analysis was investigated on five randomly selected histology sections. Histomorphometry measures were calculated by two experienced analysts using the same Matlab code for ROI drawing and semi-automatic color-based segmentation. Coefficients of variation were calculated for all results. The average coefficients of variation for area fraction, specific surface, fascicle size, and cell count were 4, 4, 3, and 5%, respectively.

2.5. Statistical analysis

Normal distribution of all MRI, histomorphometry and mechanical variables were examined using Kolmogorov-Smirnov test. All variables were found to have non-normal distributions

as expected because of the limited number of the specimens. Thus, Spearman's rank correlations were calculated between average UTE-MRI quantifications, elastic modulus, and histomorphometry measures. Correlation coefficients were used to determine the level of correlations (poor, moderate, or high[49]). All statistical analyses were performed in MATLAB. P values below 0.05 were considered as significant. Holm–Bonferroni method has been used to correct the significance level for the multiple comparisons.

3. RESULTS

Figure 2 shows single-component exponential T2*, T1, T1ρ fittings as well as an MT modeling curve for a representative ACL specimen (sample 1 in Fig.1C, from a 61-year-old male donor). Figure 2A illustrates schematically the selected ROI for MRI analysis.

Figure 3 illustrates representative histological images of AB/PAS-stained slides of four different ACL specimens. Histology sections in Figures 3A and 3C (from 88- and 27-year-old male donors, respectively) present larger fascicles compared with the histology sections in Figures 3B and 3D (from 31-year-old male and 42-year-old female donors, respectively). The average specific surface of the fascicles in ACL specimens in Figures 3B and 3D (0.0637 and 0.0603 1/μm, respectively) were higher than those in Figures 3A and 3C (0.0263 and 0.0173 1/μm, respectively).

Details of subject demographics, UTE-MRI, elastic modulus, and the histomorphometry measures distributions in studied specimens are presented in Table 2. A series of MTR values were measured, but only MTR value for 800° pulse power at 2 kHz frequency offset is presented in the table as the other MTR values showed similar trends.

The Spearman's rank correlation coefficients between UTE-MRI quantification and elastic modulus as well as histomorphometry measures of the ACL specimens are presented in Table 3. According to Holm–Bonferroni correction for the multiple comparisons, the ACL elastic modulus showed significant moderate[49] correlations with UTE-Adiab-$T_{1\rho}$ (R=−0.59, P=0.01), macromolecular fraction (MMF) from MT modeling (R=0.54, P=0.01), and UTE-T2* (R=−0.53, P=0.01). Three sets of magnetization transfer ratio including MTR-8-2 (for 800° pulse power at 2 kHz frequency), MTR-8-5 (for 800° pulse power at 5 kHz frequency), and MTR-6-2 (for 600° pulse power at 2 kHz frequency) showed significant moderate correlations with the ACL elastic modulus (R=0.53, 0.54, and 0.53, respectively, P=0.01). ACL elastic modulus also showed significant moderate correlation with average fascicle specific surface (R=0.54, P=0.01). UTE-MRI correlations with histomorphometry measures were not significant. Correlations between UTE-MRI parameters are presented in Table 2S of Supplemental Material.

The scatter plots and linear regression analyses of ACL elastic modulus on UTE-MRI measures are illustrated in Figure 1S of Supplemental Material.

Figure 4 depicts pixel maps of UTE-Adiab-T1ρ and MMF over the UTE-MRI image of the thirteen studied ACL specimens. Correlation coefficients from linear regression models were highest for UTE-Adiab-$T_{1\rho}$ and MMF (Figure 1S). ACL specimens with higher MMF on average, show much lower Adiab-T1ρ values.

4. DISCUSSION

This study was the first to focus on the assessment of human ACL mechanical and microstructural properties using quantitative 3D UTE Cones techniques (T_2*, Adiab-$T_{1\rho}$, T_1, and MTR, as well as MMF and T_2mm from two-pool MT modeling). In previous studies, UTE-Adiab-$T_{1\rho}$ and the UTE-MT measures have demonstrated low sensitivities to the magic angle effect which highlight them as potential non-invasive MRI-based biomarkers for MSK tissue assessment [35,42,44,46]. It should be noted that if the tissue orientation could be retained constantly between different MRI visits, other UTE-MRI techniques such as UTE-T2* could also evaluate MSK tissues consistently. The UTE-MT modeling technique has been investigated in previous studies on other MSK tissues and demonstrated significant correlations with bone microstructural properties [50], bone [51] and cartilage mechanical properties[52], and tendon structure [46,53]. The feasibility of UTE-Adiab-$T_{1\rho}$ employment for mechanical and structural assessment of other MSK tissues are yet to be investigated.

Our study of thirteen human ACL specimens demonstrated significant moderate correlations of elastic modulus with Adiab-$T_{1\rho}$, MMF, MTR, and T2* (Table 3). These UTE-MRI biomarkers showed non-significant correlations with the histomorphometry results. The higher MMF and MTR in the ACL specimens indicates the higher macromolecular content (collagen and proteoglycan) which expectedly results in higher mechanical properties. The higher T1ρ and T2* likely indicate more water or less structured macromolecules which can be found in the ACL specimens with lower mechanical stiffness.

It should be noted that the focus of this study has been the investigation of the correlations of UTE-MRI measures with mechanical and histomorphometry of ACL specimens. Differences in the correlation levels between studied UTE-MRI measures may change if more samples were included or other fitting models could be used such as bicomponent T2* modeling.

Elastic modulus showed significant moderate correlation with the fascicle specific surface from histomorphometry results. The higher specific surface of the fascicles may increase the contact area between fibers and fascicles (inter-fascicular contact area), which in turn is assumed to increase the integration between fascicles and fibers. Such an increased fascicle integration could lead to higher elastic modulus of the ACL as found in this study. It should be noted that both anteromedial and posterolateral fascicle bundles of the ACL were covered by the global ROIs in MRI and histological analysis. Although the fiber alignment and stiffness of the anteromedial and posterolateral fascicle bundles are different, but both fascicle bundles of the ACL were assumed to contribute similarly to the mechanical properties of the specimens in this study. The bundles were mounted evenly into the grippers, to minimize the potential disparities in the contributions of the anteromedial and posterolateral fascicle bundles to elastic modulus. Nevertheless, separating the contribution of the two bundles in performed mechanical test would be highly challenging.

Few studies have been reported investigating the correlations between the mechanical properties of ACL and the quantitative MR techniques [2,20-26]. To the knowledge of the authors, correlations between quantitative MRI and intact human ACL mechanical has been

investigated only by Biercevicz et al. [26]. They investigated T2* correlations with failure load of intact human ACL specimens harvested from 15 cadaveric knee joints from 24–76 years old donors and reported non-significant moderate correlations (R=0.48, p=0.20) [26]. Calculated correlation level between T2* and the ACL elastic modulus in the current study was slightly higher than the correlations reported by Biercevicz et al. [26]. Despite the reported non-significant correlations in the previous study, correlation in the current study was significant (Spearman's correlation test). The difference in the significance levels was likely due to the limited number of specimens in both studies, different loading rates (20 vs. 2 mm/min), comparisons with different mechanical properties (failure load of the femur-ACL-tibia specimens vs. elastic modulus of the dissected ACL specimens), using different MRI sequences (Clinical FLASH vs. UTE). Notably, quantitative MRI techniques have been used for the assessment of ACL grafts in vivo where decreasing trends of T2*, T1ρ and T2 have been reported by increasing the maturity level of the ACL grafts [20-23]. It should be noted that the ACL grafts are mostly tendon sections which possess higher T2*, T1ρ and T2 values compared with native ACL tissue.

Quantitative UTE-MRI techniques mainly evaluate tissues' composition and microstructure regardless of the specimen length and volume, which likely depend on the race, sex, and height of the subjects. Nevertheless, ACL length and volume need to be controlled in future diagnostic studies to avoid their influences on the conclusions about the diagnostic capability of the UTE-MRI techniques.

The limitations of this study can be summarized in six aspects. First, the number of samples was relatively small as is the nature of pilot studies. Moreover, the ACL specimens were from thirteen unique donors, and were without any visible abnormality such as degeneration or tearing. Inclusion of more ACL specimens with some degrees of degeneration is expected to increase the generalizability of this study. Second, the ACL specimens were dissected from tibial and femoral bone to ease MRI imaging and the corresponding comparisons between specimens. However, this does not mimic accurately the in vivo load distribution on the ligaments. Moreover, during the MRI scans, the specimens were not placed in their precise anatomical direction in the body. Nevertheless, as the specimens were all in the same direction, the orientation impact was assumed to be the same on all specimens and did not impact the correlation study presented here. Third, specimens were soaked in PBS for 2 hours before scanning to ensure similar rehydration level which may affect the quantitative MRI measures. However, the impact of the PBS soaking was assumed to be similar in all specimens and did not influence the comparisons presented in this study.

Fourth, histological analysis was performed on axial planes of the ACL specimens which limits the histomorphometry analysis to the fascicle cross-sectional microstructure and the cell counts. Adding histology in a longitudinal plane could allow for additional measurements, including characterization of fascicle crimp patterns. Furthermore, longitudinal plane histology would improve the validity of this study because the fiber bundle alignment and stiffness vary along the ligament length. Such differences in the superior, middle, and inferior portions of the specimens could be adding noise to the presented data and decreasing the reported significance level. Fifth, this study was performed on ex vivo specimens after a single freeze-thaw cycle, which may have

influenced the results. However, studies have shown that a single freeze-thaw cycle does not significantly affect biomechanical properties [54]. Furthermore, freezing was expected to affect the histological measures similarly in all specimens, therefore the correlation results may be valid. Nonetheless, a well-designed in vivo study should be performed in the future to examine the correlations between the MRI measures and the ACL mechanical properties, potentially using arthroscopic mechanical test instruments for patients undergoing knee surgeries. Sixth, reliability and repeatability levels of UTE-MRI and histomorphometry techniques were not investigated in this study. However, adequate reliability and repeatability levels were expected to be achieved for UTE-MRI and histomorphometry measurements. Specifically, we have previously performed an in vivo reproducibility investigation on bone UTE-MT-MRI and observed an average coefficient of variation (i.e., standard deviation/average) equal to 1% for MMF [55]. On the other hand, histomorphometry analysis was performed by an experienced analyst blinded to other results via a semi-automatic measurement approach.

5. Conclusions

A series of 3D UTE Cones biomarkers, including T_2*, T_1, Adiab-$T_{1\rho}$, MTR, MMF and T_2mm were investigated for their correlations with the microstructural and mechanical properties of human ACL specimens. ACL tensile elastic modulus showed significant moderate correlations with UTE-Adiab-$T_{1\rho}$, MMF from two-pool UTE-MT modeling, MTR and UTE-T2*. UTE-MRI showed non-significant correlations with histomorphometry measures. This study highlighted the potential of UTE-MRI techniques for the ACL mechanical assessment which can help improve ACL injury detection which requires further investigations.

Supplementary Material

Refer to Web version on PubMed Central for supplementary material.

Acknowledgements

The authors acknowledge grant support from NIH (R21AR073496, R01AR075825, 2R01AR062581, 1R01 AR068987), VA Clinical Science and Rehabilitation R&D Awards (I01CX001388 and I01RX002604), and JSPS KAKENHI (JP19K09658, JP18KK0104).

Abbreviations:

MR	magnetic resonance
MRI	magnetic resonance imaging
3D	three-dimensional
UTE	ultrashort echo time imaging
RF	radio frequency
FOV	field of view

ROI	region of interest
TE	echo time
TR	repetition time
MT	magnetization transfer
MTR	magnetization transfer ratio
MMF	macromolecular fraction
T_2mm	macromolecular T_2
FA	flip angle
PBS	phosphate buffered saline
AB/PAS	Alcian blue/periodic acid Schiff stain

8. References

1. Boden BP, Dean CS, Feagin JA, Garrett WE. 2000. Mechanisms of anterior cruciate ligament injury. Orthopedics .
2. Fleming BC, Biercevicz AM, Murray MM, et al. 2017. Emerging Techniques for Tendon and Ligament MRI. In: Magnetic Resonance Imaging in Tissue Engineering. p 209–236.
3. Chang EY, Du J, Chung CB. 2015. UTE imaging in the musculoskeletal system. J. Magn. Reson. Imaging 41(4):870–883 Available from: 10.1002/jmri.24713. [PubMed: 25045018]
4. LaBella CR, Hennrikus W, Hewett TE, et al. 2014. Anterior cruciate ligament injuries: Diagnosis, treatment, and prevention. Pediatrics 133(5):e1437. [PubMed: 24777218]
5. Howell SM, Knox KE, Farley TE, Taylor MA. 1995. Revascularization of a Human Anterior Cruciate Ligament Graft During the First Two Years of Implantation. Am. J. Sports Med. 23(1):42–49. [PubMed: 7726349]
6. Murray MM, kurt P. Spindle, Abreu E, et al. 2007. Collagen-Platelet Rich Plasma Hydrogel Enhances Primary Repair. J. Orthop. Res. 25(1):81–91. [PubMed: 17031861]
7. Mcfarland EG, Morrey BF, an KN, Wood MB. 1986. The relationship of vascularity and water content to tensile strength in a patellar tendon replacement of the anterior cruciate in dogs. Am. J. Sports Med. 14(6):436–448. [PubMed: 3541655]
8. Arai Y, Hara K, Takahashi T, et al. 2008. Evaluation of the vascular status of autogenous hamstring tendon grafts after anterior cruciate ligament reconstruction in humans using magnetic resonance angiography. Knee Surgery, Sport. Traumatol. Arthrosc. 16(4):342–347.
9. Figueroa D, Melean P, Calvo R, et al. 2010. Magnetic resonance imaging evaluation of the integration and maturation of semitendinosus-gracilis graft in anterior cruciate ligament reconstruction using autologous platelet concentrate. Arthrosc. - J. Arthrosc. Relat. Surg. 26(10):1318–1325.
10. Howell SM, Clark JA, Blasier RD. 1991. Serial magnetic resonance imaging of hamstring anterior cruciate ligament autografts during the first year of implantation: A preliminary study. Am. J. Sports Med. 19(1):42–47. [PubMed: 2008929]
11. Radice F, Yánez R, Gutiérrez V, et al. 2010. Comparison of Magnetic Resonance Imaging Findings in Anterior Cruciate Ligament Grafts With and Without Autologous Platelet-Derived Growth Factors. Arthrosc. - J. Arthrosc. Relat. Surg. 26(1):50–57.
12. Saupe N, White LM, Chiavaras MM, et al. 2008. Anterior cruciate ligament reconstruction grafts: MR imaging features at long-term follow-up-correlation with functional and clinical evaluation. Radiology 249(2):581–590. [PubMed: 18769016]

13. Kiekara T, Järvelä T, Huhtala H, et al. 2014. Tunnel communication and increased graft signal intensity on magnetic resonance imaging of double-bundle anterior cruciate ligament reconstruction. Arthrosc. - J. Arthrosc. Relat. Surg. 30(12):1595–1601.

14. Mutsuzaki H, Kanamori A, Ikeda K, et al. 2012. Effect of calcium phosphate-hybridized tendon graft in anterior cruciate ligament reconstruction: A randomized controlled trial. Am. J. Sports Med. 40(8):1772–1780 Available from: 10.1177/0363546512449618. [PubMed: 22713551]

15. Ma Y, Murawski CD, Rahnemai-Azar AA, et al. 2015. Graft maturity of the reconstructed anterior cruciate ligament 6 months postoperatively: a magnetic resonance imaging evaluation of quadriceps tendon with bone block and hamstring tendon autografts. Knee Surgery, Sport. Traumatol. Arthrosc 23(3):661–668.

16. Tanaka Y, Yonetani Y, Shiozaki Y, et al. 2014. MRI analysis of single-, double-, and triple-bundle anterior cruciate ligament grafts. Knee Surgery, Sport. Traumatol. Arthrosc. 22(7):1541–1548.

17. Carroll CC, Dickinson JM, Haus JM, et al. 2008. Influence of aging on the in vivo properties of human patellar tendon. J. Appl. Physiol 105(6):1907–1915. [PubMed: 18927271]

18. Biercevicz AM, Miranda DL, MacHan JT, et al. 2013. In situ, noninvasive, T2*-weighted mri-derived parameters predict Ex vivo structural properties of an anterior cruciate ligament reconstruction or bioenhanced primary repair in a porcine model. Am. J. Sports Med. 41(3):560–566 Available from: 10.1177/0363546512472978. [PubMed: 23348076]

19. Xu B, Zhang H, Li B, Wang W. 2018. Comparison of magnetic resonance imaging for patients with acute and chronic anterior cruciate ligament tears. Med. J 97(10):1–4.

20. Chu CR, Williams AA. 2019. Quantitative MRI UTE-T2* and T2* Show Progressive and Continued Graft Maturation Over 2 Years in Human Patients After Anterior Cruciate Ligament Reconstruction. Orthop. J. Sport. Med 7(8):1–10.

21. Niki Y, Yasuoka T, Kobayashi S, et al. 2019. Feasibility of T1rho and T2 map magnetic resonance imaging for evaluating graft maturation after anatomic double-bundle anterior cruciate ligament reconstruction. J. Orthop. Surg. Res 14(1):1–8. [PubMed: 30606215]

22. Lansdown DA, Xiao W, Zhang AL, et al. 2020. Quantitative imaging of anterior cruciate ligament (ACL) graft demonstrates longitudinal compositional changes and relationships with clinical outcomes at 2 years after ACL reconstruction. J. Orthop. Res 38(6):1289–1295. [PubMed: 31868948]

23. Warth RJ, Zandiyeh P, Rao M, et al. 2020. Quantitative Assessment of In Vivo Human Anterior Cruciate Ligament Autograft Remodeling: A 3-Dimensional UTE-T2* Imaging Study. Am. J. Sports Med. 48(12):2939–2947. [PubMed: 32915640]

24. Biercevicz AM, Proffen BL, Murray MM, et al. 2015. T2* relaxometry and volume predict semi-quantitative histological scoring of an ACL bridge-enhanced primary repair in a porcine model. J. Orthop. Res 33(8):1180–1187. [PubMed: 25764143]

25. Biercevicz AM, Murray MM, Walsh EG, et al. 2014. T2* MR relaxometry and ligament volume are associated with the structural properties of the healing ACL. J. Orthop. Res 32(4):492–499. [PubMed: 24338640]

26. Biercevicz AM, Akelman MR, Rubin LE, et al. 2015. The uncertainty of predicting intact anterior cruciate ligament degeneration in terms of structural properties using T2* relaxometry in a human cadaveric model. J. Biomech 48(6):1188–1192. [PubMed: 25746575]

27. Le J, Peng Q, Sperling K. 2016. Biochemical magnetic resonance imaging of knee articular cartilage: T1rho and T2 mapping as cartilage degeneration biomarkers. Ann. N. Y. Acad. Sci 1383(1):34–42. [PubMed: 27472534]

28. Wang L, Regatte RR. 2015. T1ρ MRI of human musculoskeletal system. J. Magn. Reson. Imaging 41(3):586–600. [PubMed: 24935818]

29. Wheaton AJ, Casey FL, Gougoutas AJ, et al. 2004. Correlation of T1ρ with fixed charge density in cartilage. J. Magn. Reson. Imaging 20(3):519–525. [PubMed: 15332262]

30. Li X, Han ET, Ma CB, et al. 2005. In vivo 3T spiral imaging based multi-slice T1ρ mapping of knee cartilage in osteoarthritis. Magn. Reson. Med 54(4):929–936 Available from: 10.1002/mrm.20609. [PubMed: 16155867]

31. Nishioka H, Hirose J, Nakamura E, et al. 2012. T 1ρ and T 2 mapping reveal the in vivo extracellular matrix of articular cartilage. J. Magn. Reson. Imaging 35(1):147–155. [PubMed: 21990043]
32. Jobke B, Bolbos R, Saadat E, et al. 2013. Mechanism of disease in early osteoarthritis: Application of modern MR imaging techniques - a technical report. Magn. Reson. Imaging 31(1):156–161. [PubMed: 22902064]
33. Chang EY, Du J, Iwasaki K, et al. 2015. Single- and Bi-component T2Star analysis of tendon before and during tensile loading, using UTE sequences. J. Magn. Reson. Imaging 42(1):114–120. [PubMed: 25223714]
34. Du J, Bydder GM. 2013. Qualitative and quantitative ultrashort-TE MRI of cortical bone. NMR Biomed. 26(5):489–506 Available from: 10.1002/nbm.2906. [PubMed: 23280581]
35. Ma Y, Carl M, Searleman A, et al. 2018. 3D adiabatic T1ρprepared ultrashort echo time cones sequence for whole knee imaging. Magn. Reson. Med 80(4):1429–1439. [PubMed: 29493004]
36. Ma Y, Chang EY, Bydder GM, Du J. 2016. Can ultrashort-TE (UTE) MRI sequences on a 3-T clinical scanner detect signal directly from collagen protons: freeze–dry and D2O exchange studies of cortical bone and Achilles tendon specimens. NMR Biomed. 29(7):912–917. [PubMed: 27148693]
37. Jerban S, Nazaran A, Cheng X, et al. 2017. Ultrashort echo time T2* values decrease in tendons with application of static tensile loads. J. Biomech 61:160–167 Available from: 10.1016/j.jbiomech.2017.07.018. [PubMed: 28780188]
38. Pauli C, Bae WC, Lee M, et al. 2012. Ultrashort–Echo Time MR Imaging of the Patella with Bicomponent Analysis: Correlation with Histopathologic and Polarized Light Microscopic Findings. Radiology 264(2):484–493 Available from: 10.1148/radiol.12111883. [PubMed: 22653187]
39. Shao H, Pauli C, Li S, et al. 2017. Magic angle effect plays a major role in both T1rho and T2 relaxation in articular cartilage. Osteoarthr. Cartil 25(12):2022–2030 Available from: 10.1016/j.joca.2017.01.013.
40. Chang EY, Ma Y, Du J. 2016. MR Parametric Mapping as a Biomarker of Early Joint Degeneration. Sport. Heal. A Multidiscip. Approach 8(5):405–411 Available from: 10.1177/1941738116661975.
41. Casula V, Autio J, Nissi MJ, et al. 2017. Validation and optimization of adiabatic T1ρ and T2ρ for quantitative imaging of articular cartilage at 3 T. Magn. Reson. Med 77(3):1265–1275. [PubMed: 26946182]
42. Wu M, Kasibhatala A, Ma Y jun, et al. 2020. Magic angle effect on adiabatic T1ρ imaging of the Achilles tendon using 3D ultrashort echo time cones trajectory. NMR Biomed. 30(1):1–10.
43. Wu M, Ma Y, Kasibhatla A, et al. 2020. Convincing evidence for magic angle less-sensitive quantitative T 1ρ imaging of articular cartilage using the 3D ultrashort echo time cones adiabatic T 1ρ (3D UTE cones-AdiabT 1ρ) sequence. Magn. Reson. Med 1(1):1–8.
44. Ma Y, Shao H, Du J, Chang EY. 2016. Ultrashort echo time magnetization transfer (UTE-MT) imaging and modeling: magic angle independent biomarkers of tissue properties. NMR Biomed. 29(11):1546–1552. [PubMed: 27599046]
45. Ma Y, Chang EY, Carl M, Du J. 2017. Quantitative magnetization transfer ultrashort echo time imaging using a time-efficient 3D multispoke Cones sequence. Magn. Reson. Med 79(2):692–700. [PubMed: 28470838]
46. Zhu Y, Cheng X, Ma Y, et al. 2018. Rotator cuff tendon assessment using magic-angle insensitive 3D ultrashort echo time cones magnetization transfer (UTE-Cones-MT) imaging and modeling with histological correlation. J. Magn. Reson. Imaging 48(1):160–168. [PubMed: 29219218]
47. Ma Y, Lu X, Carl M, et al. 2018. Accurate T 1 mapping of short T 2 tissues using a three-dimensional ultrashort echo time cones actual flip angle imaging-variable repetition time (3D UTE-Cones AFI-VTR) method. Magn. Reson. Med. 80(2):598–608 Available from: 10.1002/mrm.27066. [PubMed: 29314235]
48. Ma YJ, Zhu Y, Lu X, et al. 2017. Short T 2 imaging using a 3D double adiabatic inversion recovery prepared ultrashort echo time cones (3D DIR-UTE-Cones) sequence. Magn. Reson. Med 00(5):1–9 Available from: 10.1002/mrm.26908.

49. Mukaka MM. 2012. A guide to appropriate use of Correlation coefficient in medical research. Malawi Med. J 24(3):69–71. [PubMed: 23638278]
50. Jerban S, Ma Y, Wan L, et al. 2019. Collagen proton fraction from ultrashort echo time magnetization transfer (UTE-MT) MRI modelling correlates significantly with cortical bone porosity measured with micro-computed tomography (μCT). NMR Biomed. 32(2):e4045 Available from: 10.1002/nbm.4045. [PubMed: 30549338]
51. Jerban S, Ma Y, Dorthe EW, et al. 2019. Assessing cortical bone mechanical properties using collagen proton fraction from ultrashort echo time magnetization transfer (UTE-MT) MRI modeling. Bone Reports 8(2):1–8.
52. Namiranian B, Jerban S, Ma Y, et al. 2020. Assessment of mechanical properties of articular cartilage with quantitative three-dimensional ultrashort echo time (UTE) Cones magnetic resonance imaging. J. Biomech. In Press.
53. Jerban S, Ma Y, Namiranian B, et al. 2019. Age-related decrease in collagen proton fraction in tibial tendons estimated by magnetization transfer modeling of ultrashort echo time magnetic resonance imaging (UTE-MRI). Sci. Rep November(9):17974 Available from: www.nature.com/articles/s41598-019-54559-3. [PubMed: 31784631]
54. Moon DK, Woo SLY, Takakura Y, et al. 2006. The effects of refreezing on the viscoelastic and tensile properties of ligaments. J. Biomech 39(6):1153–1157. [PubMed: 16549103]
55. Jerban S, Ma Y, Li L, et al. 2019. Volumetric Mapping of Bound and Pore Water as well as Collagen Protons in Cortical Bone Using 3D Ultrashort Echo Time Cones MR Imaging Techniques. Bone 127(Oct):120–128 Available from: https://linkinghub.elsevier.com/retrieve/pii/S8756328219302224. [PubMed: 31176044]

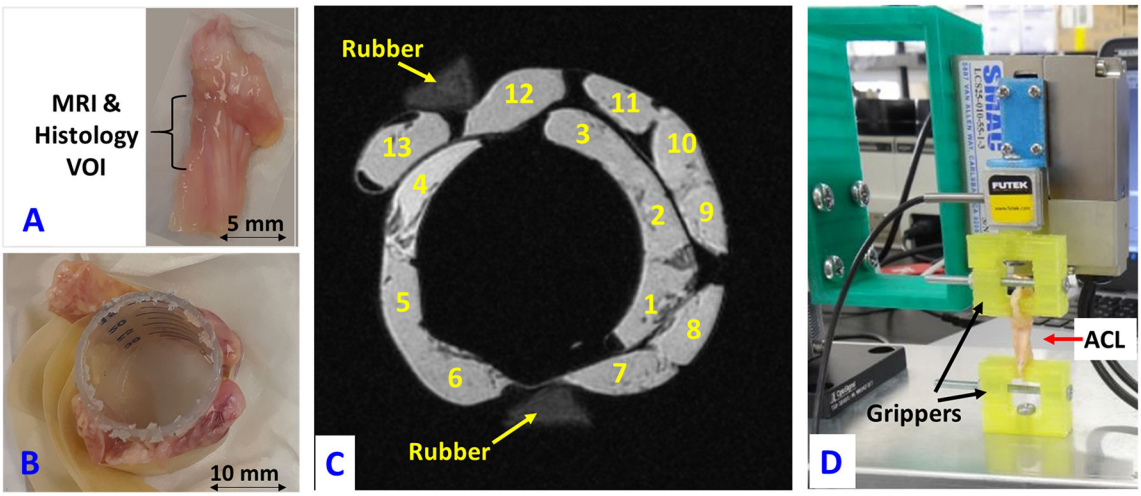

Figure 1:

(A) A representative fresh anterior cruciate ligament (ACL) specimen harvested from the knee joint of a 57-year-old male. The middle third of the specimen is highlighted as the volume interest region (VOI) analyzed in MRI and histology studies. (B) ACL specimens arranged around a sectioned portion of a standard 30-ml syringe, which was fixed with tape. (C) UTE-MRI (TE=0.032 ms, TR=500 ms, and FA=10°) image of the thirteen ACL specimens in a plastic container filled with Fomblin (with no MRI signal) imaged in the coronal plane. Two rubber phantoms are in the field of view for the purpose of orientation. (D) ACL specimen mounted on the grippers of the in-house developed benchtop uniaxial loading device for mechanical tensile tests.

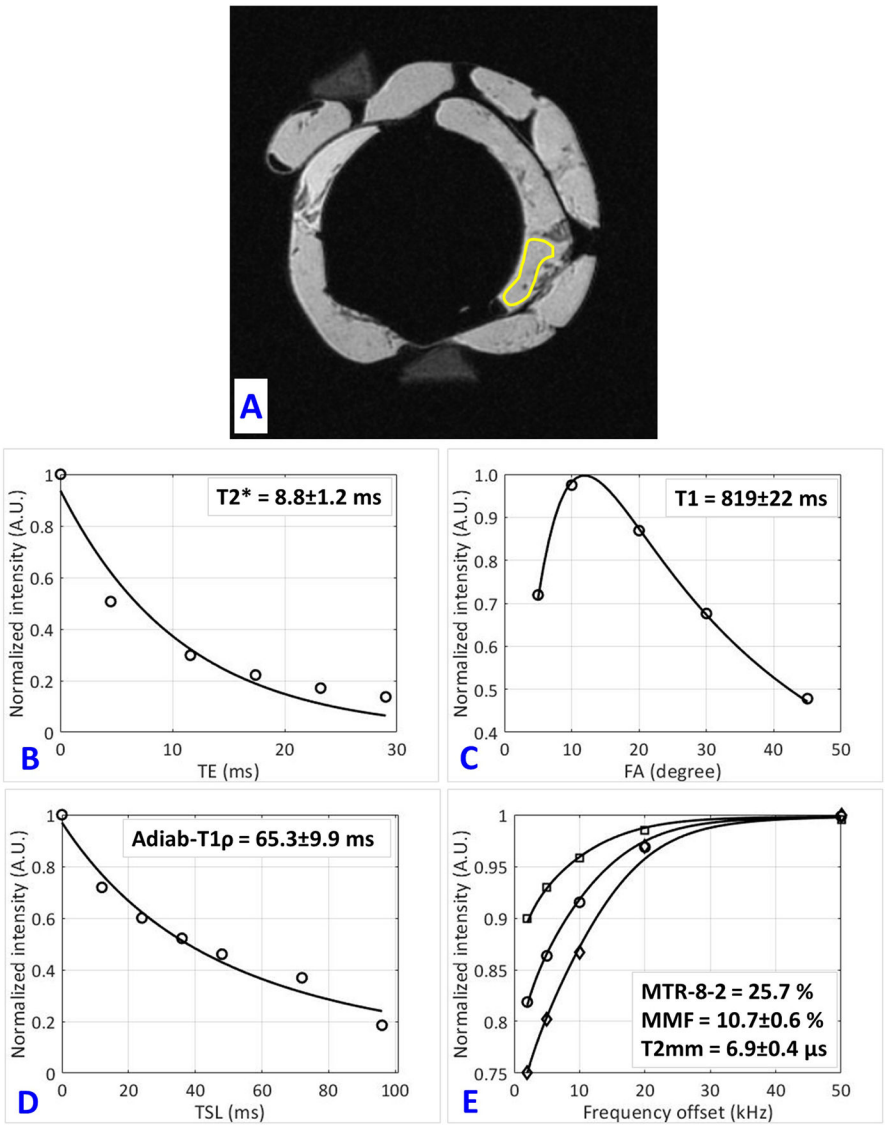

Figure 2:

Quantitative UTE-MRI analyses in a representative human ACL specimen (sample 1 in Fig.1C, from a 61-year-old male donor). (A) selected region of interest (ROI) for sample 1 depicted schematically on the UTE-MRI image. (B) Single-component exponential fitting of T2* decay, (C) T1 recovery, (D) Adiab-$T_{1\rho}$ decay (Adiab$T_{1\rho}$ signal decay vs. differing spin-lock time, TSL), and (E) two-pool MT modeling analyses in sample 1. MT modeling uses three pulse saturation powers (400°, 600° and 800°) and five frequency offsets (2, 5, 10, 20, 50 kHz). MMF and T2mm refer to macromolecular fraction and macromolecular T2, respectively.

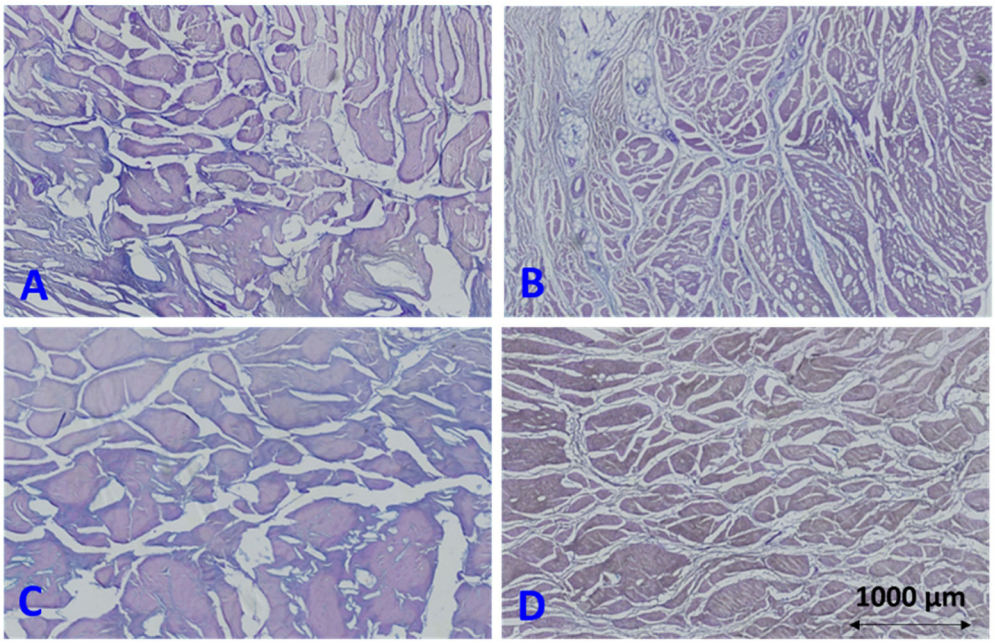

Figure 3:

Cropped histological Alcian blue/periodic-acid-schiff (AB/PAC) stain images (4×2.5 mm) of four different ACL specimens from a (A) 88-year-old male donor (sample 6 in Fig.1C), (B) 31-year-old male donor (sample 2 in Fig.1C), (C) 27-year-old male donor (sample 4 in Fig.1C), and (D) 42-year-old female donor (sample 9 in Fig.1C). Larger fascicles are observable in specimens in A and C compared with specimens in B and D. Specimens in A and C (121 and 102 kPa, respectively) presented lower mechanical properties compared with specimens in B and D (213 and 399 kPa, respectively).

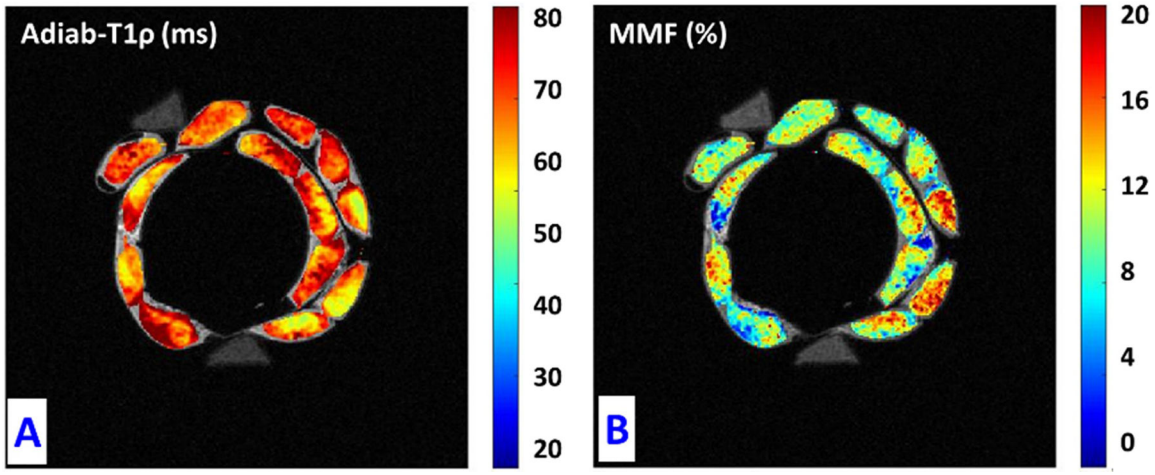

Figure 4:
(A) Adiab-T1ρ and (B) MMF pixel maps in the thirteen studied ACL specimens. Specimens with lower MMF values show higher T1ρ values.

Table 1:

Data acquisition parameters for quantitative UTE-MRI protocols.

Imaging Protocol	Sequence parameters (TR/TE/FA/TSL/θ/Δ)*	Bandwidth (kHz)	FOV (mm2)	Matrix	Slice thickness (mm)	Slice No	Scan time (min)
3D UTE Cones T2*	TR = 100 ms; FA = 10°; fat saturation; TEs=0.032, 4.5, 11.6, 17.4, 23.2, and 29.0 ms	±62.5	70×70	300×300	1	46	7
3D UTE Cones T1 (Actual flip angle, AFI Variable TR, VTR)	AFI: TE = 0.032 ms; TRs = 20 and 100 ms; FA = 45°; VFA: TE = 0.032 ms; TRs = 20 ms; FA = 5, 10, 20, 30°	±62.5	70×70	300×300	1	46	31
3D UTE Cones Adiab-T1ρ	TR = 500 ms; TE=0.032 ms, FA =10°; TSL = 0, 12, 24, 36, 48, 72 and 96 ms	±62.5	70×70	300×300	1	46	29
3D UTE Cones MT	TR = 100 ms; TE=0.032 ms, FA = 7°; θ =400°, 600°, and 800° Δ= 2, 5, 10, 20, and 50 kHz	±62.5	70×70	300×300	1	46	25

* TR: repetition time, TE: Echo time, FA: Flip angle, TSL: Spin-locking time for T1ρ, θ: Fermi saturation pulse power for MT, Δ: Frequency offset for MT

Table 2:

Average, standard deviation, and range of the UTE-MRI, mechanical and histomorphometry properties in the studied ACL specimens.

	Age (y)	T2* (ms)	T1 (ms)	Adiab-T1ρ (ms)	MMF (%)	T2mm (μs)	MTR-8,2 # (%)	E (kPa)	Area fraction (%)	Specific Surface (1/μm)	Fascicle Size (μm)	Cell count (1/mm2)
mean±SD	50.9±21.1	11.3±3.3	823±85	60.2±10.9	11.4±1.5	6.5±0.3	25.5±2.4	209±96	61.8±6.9	0.034±0.016	30.2±14.2	264±248
Min	25	6.0	650	39.6	9.7	5.9	18.8	103	48.3	0.017	10.6	2.9
Max	96	19.2	935	80.2	14.4	6.9	28.5	399	72.0	0.064	59.3	902

MTR-8,2 refers to magnetization ratio at 2 kHz frequency offset for 800° pulse power level.

Table 3:

Spearman's rank correlation coefficients between UTE-MRI and measurements from mechanical and histomorphometry analysis.

	E (kPa)	Specific surface (1/μm)	Fascicle size (μm)	Cell count (1/ mm2)
T2*	**−0.53 (p=0.01)**	−0.45 (p=0.04)	0.43 (p=0.05)	−0.09 (p=0.71)
T1	−0.33 (p=0.13)	−0.08 (p=0.76)	0.15 (p=0.51)	−0.05 (p=0.85)
Adiab-T1ρ	**−0.59 (p=0.01)**	−0.33 (p=0.13)	0.36 (p=1.00)	−0.26 (p=0.25)
MMF	**0.54 (p=0.01)**	0.22 (p=0.33)	−0.25 (p=0.27)	0.20 (p=0.39)
T2mm	−0.31 (p=0.18)	−0.17 (p=0.46)	0.12 (p=0.62)	−0.34 (p=0.13)
MTR-8,2*	**0.53 (p=0.01)**	0.25 (p=0.27)	−0.27 (p=0.22)	0.22 (p=0.33)
E (kPa)		**0.54 (p=0.01)**	−0.46 (p=0.03)	0.15 (p=0.51)

[#]MTR-8, 2 refers to magnetization ratio at 2 kHz frequency offset for 800° pulse power level.

Significant correlations are indicated with bold numbers, based on Holm–Bonferroni method